# Filter-Feeding Bivalves Store and Biodeposit Colloidally Stable Gold Nanoparticles

**ARTICLE** *in* ENVIRONMENTAL SCIENCE & TECHNOLOGY · JUNE 2011

Impact Factor: 5.33 · DOI: 10.1021/es200809c · Source: PubMed

Environmental Science & Technology

ARTICLE

pubs.acs.org/est

# Filter-Feeding Bivalves Store and Biodeposit Colloidally Stable Gold Nanoparticles

Matthew S. Hull,[†,‡,§] Perrine Chaurand,[§,∥] Jerome Rose,[§,∥] Melanie Auffan,[§,∥] Jean-Yves Bottero,[§,∥] Jason C. Jones,[†,‡] Irvin R. Schultz,[⊥] and Peter J. Vikesland[*,†,‡,§]

[†]Department of Civil and Environmental Engineering, Virginia Tech, Blacksburg, Virginia, United States

[‡]Institute for Critical Technology and Applied Science (ICTAS), Virginia Tech, Blacksburg, Virginia, United States

[§]NSF-EPA Center for the Environmental Implications of Nanotechnology (CEINT)

[∥]CEREGE, UMR 6635 CNRS/Aix-Marseille University, International Consortium for the Environmental Implications of Nanotechnology (iCEINT), Aix-en-Provence, France

[⊥]Marine Sciences Laboratory, Pacific Northwest National Laboratory, Sequim, Washington, United States

Supporting Information

**ABSTRACT:** Nanoparticles resistant to salt-induced aggregation are continually being developed for biomedical and industrial applications. Because of their colloidal stability these functionalized nanoparticles are anticipated to be persistent aquatic contaminants. Here, we show that *Corbicula fluminea*, a globally distributed clam that is a known sentinel of aquatic ecosystem contamination, can uptake and biodeposit bovine serum albumin (BSA) stabilized gold nanoparticles. Nanoparticle clearance rates from suspension were dictated by diameter and concentration, with the largest particles cleared most quickly on a mass basis. Particle capture facilitates size-selective 'biopurification' of particle suspensions with nanoscale resolution. Nanoparticles were retained either within the clam digestive tract or excreted in feces. Our results suggest that biotransformation and biodeposition will play a significant role in the fate and transport of persistent nanoparticles in aquatic systems.

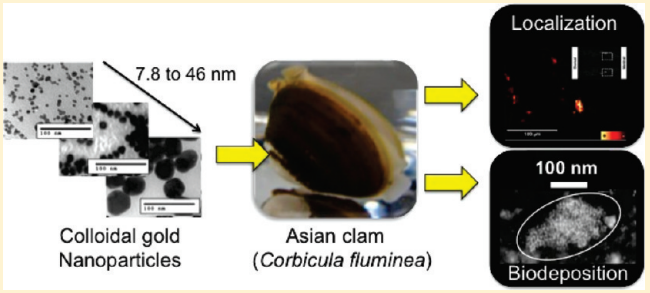


Gold nanoparticles (AuNP) are expected to be key nanoscale components in twenty-first century applications ranging from biosensors to catalysis due to their unique optical properties, chemical stability, and their capacity to exhibit a multiplicity of shapes, particle sizes, and surface chemistries.[1] Because of their increased use and chemical inertness, gold nanoparticles have potential to become a significant persistent nanomaterial input to environmental systems. To facilitate gold nanoparticle incorporation into devices and applications it is generally necessary to functionalize the nanoparticle surface with DNA, peptides, proteins, or polymers.[2−4] Serum albumin proteins such as bovine serum albumin (BSA), which are abundant in mammalian plasma, have attracted particular interest as stabilizers given their frequent use in the development and study of emerging bionanomaterials,[5] their ability to stabilize nanoparticles for cellular targeting,[6] and the propensity for nanoparticles to associate with proteins both within cells[7] and in environmental media.[8] Although the extent to which the use of BSA, specifically, will be adopted by industry remains unknown, the use of BSA as a surrogate protein for the preparation of biological macromolecule-nanoparticle conjugates is well established.

Given what we currently know about the persistence and toxicity of pharmaceutical compounds in the environment, the safe use and disposal of nanoscale particles, particularly certain types of nanomedicines functionalized for stability in highly saline media such as blood,[9,10] inherently requires efforts to understand how primary particle size and surface functionalization alter nanoparticle uptake and fate in biological and environmental systems. The objective of the present work was to investigate the size-dependent uptake, fate, and biotransformation of BSA-coated gold nanoparticles by the filter-feeding bivalve *Corbicula fluminea*. Freshwater and marine bivalves are commonly employed as biological sentinels[11] for the detection and monitoring of a broad spectrum of environmental contaminants such as metals,[12] biocides,[13] asbestos fibers,[14] bacteria,[15] and protozoan parasites.[16,17] Recently, researchers have demonstrated that biofilms and clams were the primary biological compartment for surfactant-stabilized gold nanorods added to estuarine mesocosms[18] and that 10 nm amine-functionalized gold nanoparticles penetrated the gills and digestive epithelia of *C. fluminea*.[19] The present work goes further in demonstrating the role of particle size on the rate of particle clearance

**Received:** March 10, 2011
**Accepted:** June 14, 2011
**Revised:** June 9, 2011
**Published:** June 14, 2011

from suspension and the importance of biodeposition to cross-media transference of colloidal particles.

## EXPERIMENTAL SECTION

**Preparation of Gold Nanoparticle Suspensions.** Bovine serum albumin-coated gold nanoparticles (BSA-AuNP) were prepared by incubating citrate-stabilized gold nanoparticles (citrate-AuNP) with 0.1 mg BSA-mL$^{-1}$ using established protocols.[20] Citrate-AuNP of 7.8 and 15 nm diameter were prepared as described by Jana et al.[21] and by Turkevich, respectively.[22] The seed-mediated process of Frens[23] was used to prepare 46 nm citrate-AuNP. Each suspension incorporated citrate as a reducing agent (or coreducing agent) and surface stabilizer, as citrate is known to play an important role in determining the size and monodispersivity of gold nanoparticles by regulating the pH of the reaction.[24] All suspensions were sterile-filtered (0.2 $\mu$m) and stored in an amber glass vial at 4 °C until use.

**Characterization.** Gold nanoparticle suspensions were characterized by UV−vis spectroscopy, transmission electron microscopy (TEM), and dynamic light scattering (DLS). Primary particle size and morphology were characterized using a Zeiss 10CA Transmission Electron Microscope (60 kV) equipped with a high resolution (1024 × 1024 pixel format) MT Advantage GR/HR-B CCD Camera System (Advanced Microscopy Techniques Corporation). For sample preparation, 10−20 $\mu$L of citrate- or BSA-AuNP suspension were pipetted onto a carbon-coated copper TEM grid (Electron Microscopy Sciences) and dried at room temperature. Electron micrographs were digitized and analyzed using ImagePro (MediaCybernetics, Bethesda, MD) to assess the heterogeneity of the nanoparticle suspensions and to calculate average primary particle diameters. A FEI Titan 300 operating at 200 kV was used to acquire high-resolution TEM as well as scanning tunneling electron microscopy (STEM) images. Characterization results for gold nanoparticle suspensions are provided in the Supporting Information (Table S1).

**Nanoparticle Clearance Assays with *C. fluminea*.** Adult Asian clams (*Corbicula fluminea* [Müller]) were collected from the New River near Radford, VA, and acclimated to laboratory conditions for 14 d prior to testing. *C. fluminea* nanoparticle clearance assays were performed in moderately hard, synthetic (MHS) freshwater. For studies investigating the size-dependent clearance of BSA-AuNP by *C. fluminea*, as well as the localization of BSA-AuNP within *C. fluminea* organ systems, exposures were performed in 10 L polypropylene aquariums filled with 2 L of BSA-stabilized gold nanoparticle suspension prepared in EPA MHS at a concentration of 2 mg L$^{-1}$ as Au (BSA-AuNP were stable in EPA MHS throughout the exposure period as determined by UV−vis measurements of control samples). At 2 mg L$^{-1}$, the concentrations of BSA-AuNP investigated in the current study exceed nanoparticle concentrations likely to occur in real-world environmental systems. The elevated concentration, however, was necessary to monitor colloidal stability of the BSA-AuNP suspension by UV−vis spectroscopy analysis of the surface Plasmon resonance band (SPR) throughout the duration of the assay. The authors considered the ability to monitor long-term colloidal stability to be of key importance during the current study, and thus exposures at concentrations in excess of environmentally relevant concentrations were used. To each aquarium, 75 *C. fluminea* of 1−2 years of age, 15 ± 0.6 mm in length (umbo to ventral margin), and 2.0 ± 0.3 g whole body wet weight were added at $t_0$ hours. Aquariums were continuously aerated using a borosilicate pipet. To investigate the effects of initial ($t_0$) Au concentration (2, 4, or 8 mg L$^{-1}$ as Au) on BSA-AuNP clearance, additional assays were performed in replicate 50 mL glass beakers ($n$ = 5), each of which contained 40 mL of test suspension. Individual *C. fluminea* test organisms were added to each beaker. All exposures were performed at 20 ± 1 °C. To reduce system complexity, feeding was withheld during all particle clearance assays.

Optical absorbance and water column gold concentration were monitored by UV−vis and ICP-MS, respectively. At each of the following time-points, a 1 mL water column sample was taken: 0 (control, prior to addition of organisms to test suspension), 12, 36, 60, 84, 108, and 180 h. After 180 h, *C. fluminea* were removed from the BSA-AuNP exposure, rinsed with ultrapure water, and transferred to 10 L polyethylene aquariums containing 2 L of EPA MHS diluent only (i.e., no BSA-AuNP were present in the depuration tanks). After the transfer to fresh diluent, sampling resumed and 1 mL water samples were removed at each of the following time points: 204, 228, 252, and 348 h after the experiment began. For each 1 mL sample removed from the aquarium, absorbance from 300 to 800 nm was measured. The same sample was then transferred to a sterile polystyrene tube, acidified with 200 $\mu$L aqua regia (1:3, Trace metal grade $HNO_3$:HCl), and brought to a final volume of 10 mL with ultrapure water. Samples then were analyzed for gold content by ICP-MS per Standard Method 3125-B.[25] Samples and calibration standards were prepared in a matrix of 2% aqua regia, which was more effective at dissolving the AuNP than either $HNO_3$ or HCl alone.

**Micro X-ray Fluorescence Spectroscopy ($\mu$-XRF).** At each sampling point described previously for the water column samples, three *C. fluminea* were removed from each aquarium, euthanized, and prepared for $\mu$-XRF measurements. To facilitate shell opening, interior and posterior ligaments of *C. fluminea* were severed using a surgical scalpel. Next, the interior soft tissue was dissected intact from each half-shell and rinsed three times with deionized water. The soft tissue was then placed whole into a labeled plastic tissue cassette with foam absorbent pad. The tissue samples were prepared for $\mu$-XRF analysis using a procedure described by Laforsch and Tolldrian[26] for $\mu$-XRF analysis of *Daphnia magna*. Briefly, the samples were dried in a graded series of acetone solutions (70 to 100%) before being transferred to a solution of 1,1,1,3,3,3 hexamethyldisilazane (HMDS). After 30 min in HMDS, tissue samples were transferred to a vacuum desiccator and dried overnight.

All $\mu$-XRF measurements were carried out at the lab-scale on a microscope (XGT$^{7000}$, Horiba Jobin Yvon) equipped with an X-ray guide tube producing a finely focused and high-intensity beam with a 100 $\mu$m spot size (Rh X-ray tube, accelerating voltage of 50 kV, current of 1 mA). X-ray emission from the irradiated sample is detected via an energy-dispersive X-ray (EDX) spectrometer equipped with a liquid-nitrogen-cooled high purity Si detector. Elemental maps and microanalyses were performed on HMDS-prepared whole-animal samples at atmospheric pressure. Images were obtained from the intensity of the Au L$\alpha$1 emission line. The selected region of interest (ROI) of this line was reduced in energy because of the partial overlap of the Zn K$\beta$ line with the Au L$\alpha$1 line. Moreover the background contribution was removed. The average XRF spectrum for each whole organism was generated from hyperspectral mapping (i.e., a full XRF spectrum recorded at each and every pixel of the element image) and converted to semiquantitative results (relative mass percent) using the fundamental parameters approach (FPA).

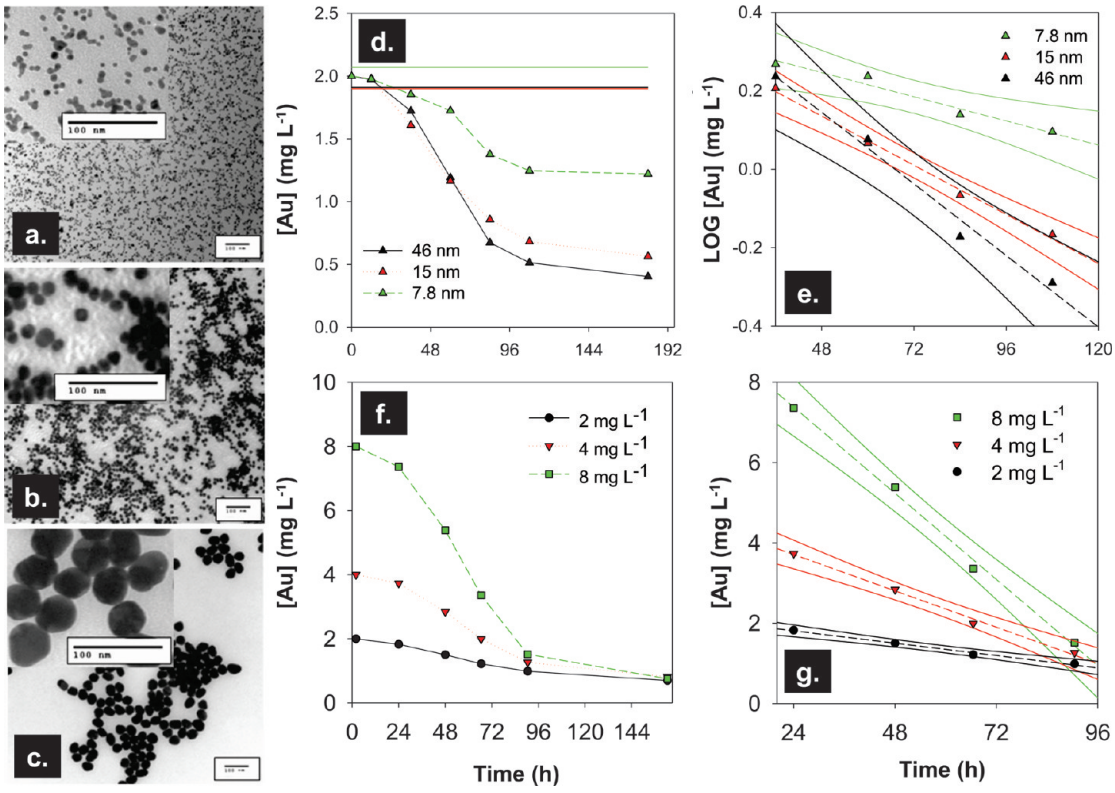


**Figure 1.** (a-c) TEM images of 7.8, 15, and 46 nm AuNP—in each panel, scale bars denote 100 nm; insets show particles at increased magnification. (d) Plot showing the average water column concentration of 7.8, 15, and 46 nm BSA-AuNP expressed in terms of Au mass concentration (mg $L^{-1}$) from 0 to 180 h (solid lines denote the average water column [Au] in negative controls—no clams present—as determined from $Abs_{SPR}$), and (e) corresponding plot of the log-transformed data (and 95% confidence intervals) for the linear clearance phase (from 48 to 120 h). (f) Plot of the average water column concentration of 46 nm BSA-AuNP as a function of [Au] at $t_0$ and time exposed to *C. fluminea*; and (g) plot of the linear phase of BSA-AuNP clearance (and 95% confidence intervals). Fitting of these data was used to determine first-order rate constants for clearance of BSA-AuNP as a function of primary particle size and [Au] concentration at $t_0$.

For enhanced sensitivity and spatial resolution (3 $\mu$m × 3 $\mu$m), $\mu$-XRF measurements were also performed on LUCIA beamline at the SOLEIL synchrotron (Paris, France) under vacuum, with a Si(111) monochromator and a silicon drift detector.[27] Due to the high intensity of the P (K) phosphorus signal compared to the Au $M_3$-edge (2743 eV), the Au map is presented as the ratio of the normalized Au map over the normalized P map.

Following $\mu$-XRF measurements, Au body burdens were determined by ICP-MS of digestates prepared by nitric acid microwave digestion of the tissue amalgamated from three clams removed at each exposure time-point (CEM MARS method #375). To ensure the complete solubilization of AuNP, 200 $\mu$L aqua regia was mixed with tissue digestates prior to analysis by ICP-MS, as described previously for water column samples. Body burdens for Au were expressed as the mass of Au (mg) per mass of wet tissue (kg).

**Characterization of Clam Feces.** Upon termination of the exposures, visible feces were harvested from each aquarium by pipet and transferred to glass scintillation vials. Up to 5 mg of each fecal sample then was transferred to an ultrathin carbon film/holey carbon 400 mesh copper TEM grid and dried overnight at room temperature. Samples were imaged by TEM, HRTEM, and STEM.

## RESULTS AND DISCUSSION

Suspensions of three different sizes of BSA-stabilized gold nanoparticles (BSA-AuNP; Figure 1a-c) were added at a mass-normalized concentration of 2 mg $L^{-1}$ (as Au) to aquariums containing seventy-five *C. fluminea* test organisms. After 180 h, *C. fluminea* filtered and removed from suspension BSA-AuNP of 7.8, 15, and 46 nm diameter (Figure 1d-e). Clearance of BSA-AuNP from the water column was quantified by daily monitoring of the total gold concentration by ICP-MS and the optical absorbance at the surface plasmon resonance band ($Abs_{SPR}$) by UV−vis spectroscopy. Over the 180-h exposure period, both [Au] and the SPR band (Supporting Information Figure S1) steadily decrease for samples from aquariums containing *C. fluminea*, but remain stable in the absence of test organisms (Figure 1d). Integrating these two measurement techniques provides a means to precisely determine concentration (in terms of total gold as measured by ICP-MS), while simultaneously providing evidence that the gold is present in nanoparticulate form (as indicated by a distinct SPR band between 500 and 550 nm that is absent for ionic gold; Supporting Information Figure S2). The location, intensity, and width of the SPR band are indicative of particle size, shape, concentration, and sample heterogeneity.[28] The initial SPR band location is a function of particle size, with the smallest particles exhibiting a hypsochromic (blue) shift of the SPR band relative to larger particles. For each particle suspension, the change in $Abs_{SPR}$ correlates with ICP-MS measurements of the total gold concentration indicating that the gold exists primarily as discrete nanoscale particles. This result is consistent with the findings of others who have reported that $Abs_{SPR}$ can be used to quantify the concentration as well as the size of noble metal nanoparticles in suspension.[28]

The absence of a measurable red-shift or significant broadening of the SPR peak between 600 and 800 nm during the exposure indicates that particle removal from suspension was not the result of particle aggregation and settling (Supporting Information Figure S3).[29,30] This absence provides clear evidence that *C. fluminea* removes discrete, BSA-stabilized nanoparticles from suspension through filtration. It is important to differentiate between these processes since, as noted by others,[31] many studies of nanoparticle uptake and toxicity fail to account for aggregation processes that result in the removal of particles from suspension due to settling and not organismal uptake.

Clearance of each size particle follows a logarithmic pattern: a lag-phase during the first 12 h of exposure, a linear clearance phase between 12 and 108 h, and a leveling off between 108 and 180 h (Figure 1d). Other researchers have shown that the filtration rates of disturbed bivalves are reduced more than 4-fold relative to undisturbed animals,[32] thus suggesting that the initial lag-phase is attributable to the acclimation period required for the clams to begin filtering following transfer to the assay chamber. The linear clearance phase is representative of a period during which the clams have acclimated to the assay environment and begun actively filtering. The leveling off observed may be the result of a combination of factors including decreasing particle concentration, gill clogging,[32] compaction of the digestive tract,[33] or physiological adjustment of filtering[34] and ingestion rates.[35] We cannot presently exclude the possibility that *C. fluminea* is initially stimulated by free or surface adhered BSA protein or that the clams preferentially deplete the BSA protein fraction and then decrease filtration activity once the ratio of BSA to AuNP is reduced below some threshold. A similar phenomenon has been reported by researchers who observed stimulated feeding behavior for *Sphaerium* and *Dreissena* bivalves exposed to high concentrations of inorganic graphite particles of 0.5 to 1.5 $\mu$m diameter;[36] in these experiments, measured filtration rates were initially very low but increased upon addition of the algal cells on which these bivalve genera commonly feed. The increase in feeding rates could be attributable to either a) facilitated uptake of graphite particles sorbed to algal cells or b) the availability of a preferred food source—in this case, algal cells. Additional studies to test the hypothesis that the presence of proteins and other biological macromolecules may stimulate uptake of BSA-AuNP are required to truly address this question. Such studies were outside the scope of the present investigation.

Clearance of BSA-AuNP during the linear-uptake phase ($12 \leq t \leq 180$ h) followed first-order kinetics and rate constants determined for the 7.8, 15, and 46 nm nanoparticles were 0.0026, 0.0052, and 0.0076 $h^{-1}$, respectively (Figure 1e). Plotting the particle clearance rate constant versus the primary particle diameter shows that the rate increases logarithmically with particle diameter (Supporting Information Figure S4). Although descriptive across the range of particle sizes studied here, this general pattern of clearance as a function of particle size does not extend to larger micrometer-sized particles, which can be cleared from suspension with 100% efficiency in less than one hour.[37] This result is not surprising, since the mechanisms used to capture particles varying so greatly in size differ due to particle fluid dynamics, composition, density, and geometry.[38]

Particle removal efficiencies,[37] calculated based on the change in the Au mass concentration between $t_0$ and $t_{180}$ indicate that 7.8, 15, and 46 nm BSA-AuNP were removed from suspension with 39, 72, and 80% efficiency, respectively. Others have demonstrated this positive correlation between the retention efficiency and the particle size with diameters as low as 2 $\mu$m.[37] Our results show that this correlation remains even at the submicrometer scale with particles differing in diameter by less than 30 nm. However, our assays with nanoscale particles require clearance periods of up to 180 h, whereas the retention efficiencies of larger micrometer-sized particles are typically determined in assays of less than an hour duration to minimize the confounding effects of gravitational settling.[37] Given the colloidal stability of BSA-AuNP in the absence of the clams (Figure 1d), gravitational settling was not a concern here.

Uptake experiments performed with 46 nm BSA-AuNP at differing initial ($t_0$) concentrations of 2, 4, and 8 mg $L^{-1}$ indicate that particle concentration also influences the rate of nanoparticle clearance from suspension (Figure 1f-g). A logarithmic clearance pattern was again evident for each initial concentration, with a lag-phase of 24 h preceding a linear decrease in the water column concentration for the next 65−70 h and then a leveling off over the final 70 h of the assay. Nanoparticle clearance during the linear-phase followed first-order kinetics and as expected for a first-order process there is a positive relationship between the initial concentration of BSA-AuNP and the clearance rate (Figure 1g). Previous research using micrometer-sized particles has shown a similar positive relationship between particle concentration and filtration rate as *Corbicula* are thought to physiologically adjust filtration rates to achieve an optimal rate of particle clearance.[34] Our data suggest that this relationship extends to particles well into the nanodomain.

**Size-Selective Sorting of Nanoscale Particles by Clams.** The size-selective clearance of BSA-AuNP observed for *C. fluminea* introduces the possibility of using bivalves or other suspension feeders to sort nanoscale particles by size with nanometer resolution. To test this hypothesis, a size-selective uptake experiment was performed using three sizes of BSA-AuNP added to 50 mL assay chambers both separately and in a combined 'cocktail'. All particle concentrations were mass normalized to give a final in-chamber gold concentration of 15 mg $L^{-1}$; for the cocktail this required adding each of the three suspensions at concentrations of 5 mg $L^{-1}$. A relatively high concentration was necessary to facilitate monitoring of the location and height of the SPR band by UV−vis spectroscopy. Suspensions could not be normalized by particle number or surface area since the mass concentrations required to achieve this for the smallest particle suspensions were below instrument detection limits.

Despite the increased $t_0$ concentration, BSA-AuNP of all three sizes were readily cleared from suspension by *C. fluminea* (Supporting Information Figure S5). Although the same positive relationship between clearance rate and particle diameter that was observed in the large-scale aquarium exposures was evident once again, quantitative comparisons among the rate constants obtained from these two experiments are not possible due to differences in Au concentration, water volume, and number of test organisms. After 120 h the mean SPR band for the cocktail to which clams were added blue-shifted ≈4 nm, suggesting a decrease in the average particle diameter (Supporting Information Figure S6a). The difference between the location of the SPR band of the cocktail in the presence and absence of the clams was greatest after 72 h (Supporting Information Figure S6a), suggesting that a practical application of filter-feeding organisms to size-purify nanoparticles would require an exposure duration that achieves maximum size-reduction without allowing excreted metabolites to reach levels that might induce particle aggregation through alteration of solution ionic strength or pH.

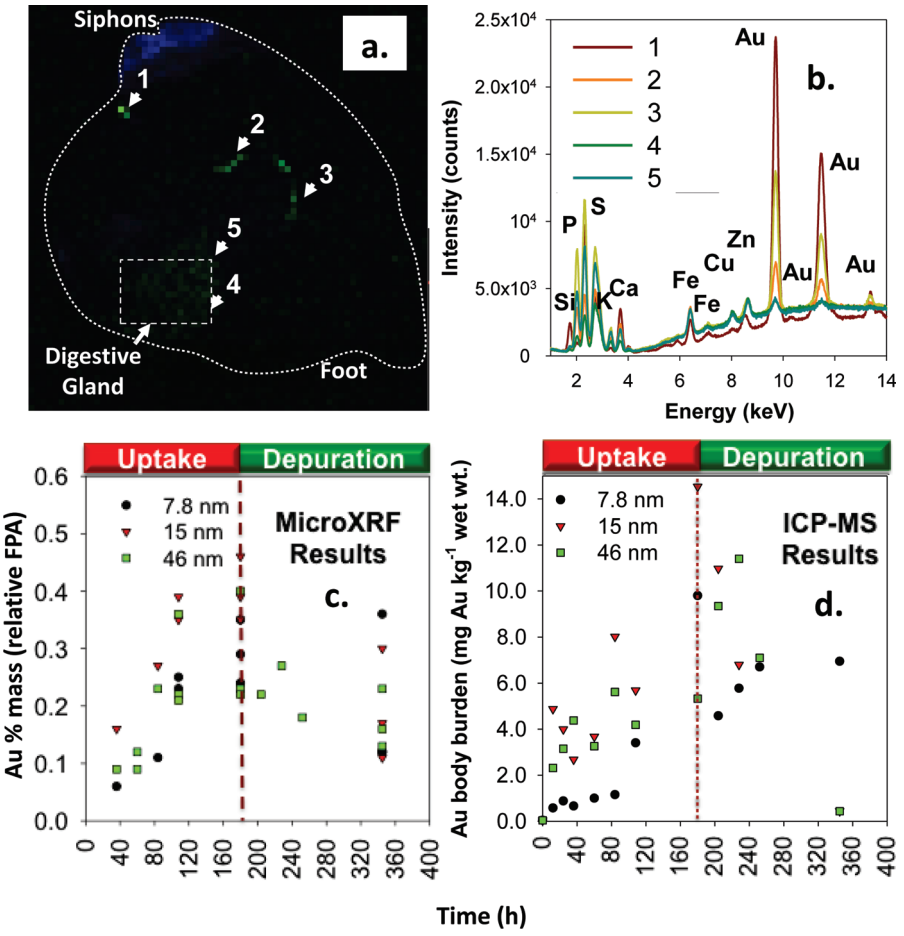


**Figure 2.** (a) A $\mu$−XRF image of an HMDS-fixed *C. fluminea* specimen exposed to 46 nm BSA-AuNP for 180 h. Siphons, which were rich with Fe, are colored blue; Au-rich regions in the intestine and at the anus are colored green. The body of the organism is encircled by a dashed line, and the locations of the siphons and foot are noted; a dashed rectangle surrounds the digestive gland—additional analysis of the digestive gland and organism cross sections are provided in the Supporting Information (Figure S8). (b) Semiquantitative data of the elemental composition of samples were collected by $\mu$-XRF spot-analysis of the *C. fluminea* specimen shown in panel (a), with numbers 1−5 corresponding to the Au-rich locations noted on the $\mu$-XRF image. Plots showing (c) the relative Au composition (%) of HMDS-fixed *C. fluminea* as determined by $\mu$-XRF and (d) Au body burden (mg Au $kg^{-1}$ wet tissue weight) as determined by ICP-MS of acid-digested tissue as a function of time (0 to 345 h) and primary particle size of BSA-AuNP—7.8, 15, and 46 nm. The vertical dashed lines at 180 h (panels c and d) indicate the point at which *C. fluminea* were rinsed and transferred from the BSA-AuNP test suspensions to fresh EPA MHS water and allowed to depurate their gut contents.

Based on the clearance rates of the individual particle suspensions, after 120 h filtering by *C. fluminea*, the relative percent composition (by mass) of the cocktail changed from being divided evenly at one-third for each particle size to being more than one-half 7.8 nm particles (Supporting Information Figure S6b). The optical absorbance of the largest particles, 46 nm, was reduced to below the detection limits of the UV−vis after 96 h, suggesting that these particles likely comprised less than 10% of the cocktail upon termination of the experiment. It is worth noting that the SPR shift of ~4 nm could be replicated experimentally by preparing cocktails corresponding to the measured gold concentrations and predicted particle size distributions at $t_0$ and $t_{120}$ during the size-selective uptake assay (Supporting Information Figure S7).

Although not previously reported for nanoscale particles, investigators have noted that bivalves filter or retain small particles less efficiently than larger particles, and thus the fraction of these "inefficiently retained" particles can increase over time.[32] Other researchers have suggested that small particles, typically <3 $\mu$m in diameter, exhibit 'negative retention' in studies of particle retention by bivalves.[37,39,40] A conspicuous lack of particle characterization in conjunction with these uptake studies, however, has limited the ability of investigators to draw definitive conclusions as to the source and composition of these particles. At least one researcher concluded that small particles were produced by bivalve test organisms,[37] whereas more recently, others have concluded that such particles do not necessarily originate from the study organisms.[41] Our results suggest that on a mass basis, the efficiency with which filter-feeding bivalves clear particles from the water column decreases with a decrease in particle diameter, even in the nanometer domain, and this may facilitate the biologically mediated separation of particles differing in size by only tens of nanometers. Clearance rates for particles of 7.8 and 15 nm diameter, while generally indistinguishable from one another, could be differentiated from the largest diameter particles (46 nm). In theory, such biologically mediated size-selection of colloidal particles could be applied as a potentially low-cost, passive, and continuous alternative to conventional size purification techniques such as differential centrifugation or tangential flow filtration. Additional studies are required, however, to realize

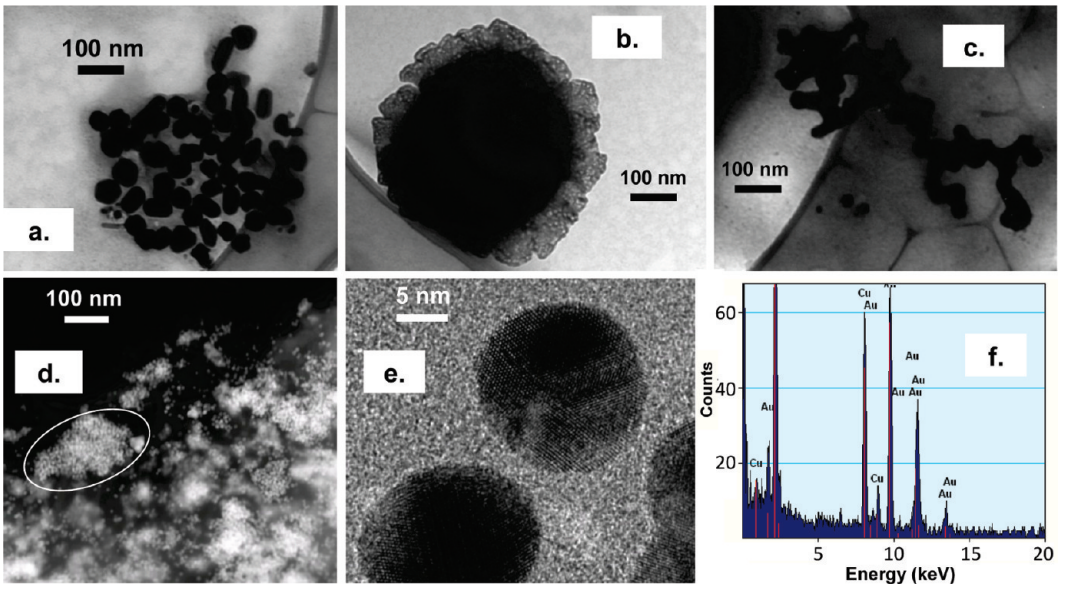


**Figure 3.** TEM images showing structures recovered from feces egested by *C. fluminea* following exposure to BSA-AuNP at 2 mg $L^{-1}$ as [Au]: (a) cluster of AuNP that are less spherical and less uniform in size than the 46 nm BSA-AuNP that were originally dosed to clams; (b, c) two different types of aggregate structures recovered from the same fecal sample; (d) STEM image of low electron-density fecal material containing clusters of 15 nm AuNP (white circle added to indicate one cluster); (e) Hi-Res TEM and (f) EDX indicating that particles recovered from feces of clams exposed to 15 nm BSA-AuNP at 2 mg $L^{-1}$ are spherical, crystalline, uniform in size, and comprised primarily of Au.

any practical application of this concept, as a number of factors ranging from the condition of the filtering organisms to the presence of stabilizers or preservatives that may co-occur with commercial nanomaterials will likely influence actual filtration rates.

**Fate and Biotransformation of Nanoparticles in Bivalves.** Analysis of whole−organism, soft-tissue preparations (shells removed) by X-ray fluorescence microscopy ($\mu$-XRF) indicated that gold was confined to the digestive gland and regions of the digestive tract of BSA-AuNP-exposed *C. fluminea* with little indication of migration to other organ systems (Figure 2a,b). Because $\mu$-XRF does not discriminate between surface-associated versus internalized analytes, analyses of organism cross sections were performed and verified that gold was internalized and not simply sorbed to the external surfaces of the organisms (Supporting Information Figure S8a). These cross sections were also analyzed using the synchroton-based XRF microscope LUCIA with a beam size of 3 $\mu$m × 3 $\mu$m. With this improved sensitivity and spatial resolution, we observed spots of gold that are diffusely distributed throughout the digestive gland. The larger clusters are about 15 × 30 $\mu$m, and most of them are below 3 to 6 $\mu$m (Supporting Information Figure S8b). We note that $\mu$-XRF cannot differentiate between nanoparticulate gold or soluble gold; however, because nanoparticulate gold was observed in collected feces (*vide infra*) we expect that the gold signal from the digestive system is primarily due to nanoparticulate gold.

The gold content of whole *C. fluminea* was evaluated using a combination of $\mu$-XRF and the fundamental parameters approach (FPA).[42] The obtained percent mass as Au correspond to semiquantitative and relative values and are plotted as a function of time (Figure 2c). These results show that exposed clams contained gold, particularly in the digestive gland and at regions along the digestive tract (Figure 2a,b) and that the relative mass concentration of gold increased as a function of time for each particle size until the clams were removed from the BSA-AuNP exposure after 180 h and transferred to clean water (Figure 2c). For each particle size, the rate of increase in the relative mass concentration of gold measured in *C. fluminea* tissue was most rapid over the first 108 h of the exposure, which corresponds with the period of most rapid particle clearance from suspension. At each measured time-point during the accumulation phase, the relative mass concentration of gold present in the clams exposed to 15 nm BSA-AuNP was consistently greater than for the other two particle sizes, but this relationship was not statistically significant. In contrast to the $\mu$-XRF results, but in strong support of the suspension chemistry results showing reduced clearance rates for the smallest particles (Figure 1d,e), ICP-MS analysis of tissue digestates show that the mass of Au internalized by *C. fluminea* via filtering of 7.8 nm BSA-AuNP was dramatically reduced relative to that of the 15 and 46 nm particles (Figure 2d). Discrepancies in $\mu$-XRF and ICP-MS measures of Au were expected, however, since $\mu$-XRF of whole-organism samples is sensitive to variations in three-dimensional sample geometry and subsequent fluctuations in X-ray penetration and fluorescence, whereas ICP-MS is not subject to these same influences.

Following the transfer of clams to clean water, tissue gold concentrations determined by $\mu$-XRF decreased but, even after 165 h, did not return to pre-exposure levels (Figure 2c). Tissue Au concentrations measured by ICP-MS, however, indicated a return to near-background levels for 15 and 46 nm BSA-AuNP, whereas Au levels remained elevated for clams exposed to the 7.8 nm particles (Figure 2d). As suggested by others who recently compared the uptake of aggregated versus disaggregated nanoparticles by *Mytilus edulis* and *Crassostrea virginica*,[43] extended retention times in the gut may be indicative of particles undergoing extracellular digestion processes, and our results support this contention.

Semiquantitative $\mu$-XRF data suggest that clams partially accumulate and retain gold in the digestive tract and gland but provide only limited information about the form that gold nanoparticles take during digestion. If *C. fluminea* are capable

of digesting gold nanoparticles, then changes in particle size, shape, or aggregation state should be expected. Examination of fecal material by Scanning Tunneling Electron Microscopy (STEM) and High-Resolution Transmission Electron Microscopy (HRTEM) coupled with Energy Dispersive X-ray Spectroscopy (EDX) indicate that particles can be recovered from *C. fluminea* feces in a variety of forms, including nanoscale aggregates and individual particles (Figure 3a-e), and that feces are comprised of a mixture of electron-dense metals including Au (Figure 3f). For the 46 nm BSA-AuNP, nanoparticles recovered in feces appeared much less spherical and uniform in size than prior to the exposure (Figure 3a), suggesting that some dissolution or mechanical alteration of the particles had occurred as a result of digestion and excretion. Conversely, 15 nm BSA-AuNP were recovered in fecal materials in dense clusters of particles (Figure 3d) but retained their spherical shape and uniform size (Figure 3e). These results confirm that filter-feeding bivalves likely will play an important role in transforming and transferring nanoscale particles suspended in the water column to the subsurface via biodeposition. Biodeposition, or the process of filtering, compacting, and depositing suspended particulate matter at the sediment-water interface, is an important ecological function performed by both freshwater and marine bivalves as well as many other suspension feeders, and in some aquatic systems, the magnitude of this process can exceed tens of thousands of metric tons of biodeposited material annually.[44]

## ■ ASSOCIATED CONTENT

**Supporting Information.** Time-dependent clearance of BSA-AuNP suspensions as measured by UV−vis spectroscopy, extinction spectra for BSA-AuNP of varying diameter, comparison of UV−vis spectra for aggregating AuNP versus AuNP that have been cleared from suspension via biological filtration, comparison of SPR band shifts for AuNP cocktails with or without clams present, and a summary of physicochemical properties for BSA-AuNP. This material is available free of charge via the Internet at http://pubs.acs.org.

## ■ AUTHOR INFORMATION

**Corresponding Author**
*E-mail: pvikes@vt.edu.

## ■ ACKNOWLEDGMENT

We are grateful for funding from the US National Science Foundation (BES 0853989) and the Virginia Tech Institute for Critical Technology and Applied Science. This material is based upon work supported by the National Science Foundation (NSF) and the Environmental Protection Agency (EPA) under NSF Cooperative Agreement EF-0830093, Center for the Environmental Implications of NanoTechnology (CEINT). Any opinions, findings, conclusions, or recommendations expressed in this material are those of the authors and do not necessarily reflect the views of the NSF or the EPA. This work has not been subjected to EPA review, and no official endorsement should be inferred. W. Miles, R. Davis, R. Elston, M. Muryama, and K. Lowe provided invaluable assistance with sample characterization. We are grateful to the SOLEIL synchrotron (Paris, France) for the provision of beam time and acknowledge LUCIA staff (Nicolas Trcera, Anne-Marie Flank) for their technical support during data collection.

## ■ REFERENCES

(1) Daniel, M.; Astruc, D. Gold nanoparticles: assembly, supramolecular chemistry, quantum-size-related properties, and applications toward biology, catalysis, and nanotechnology. *Chem. Rev.* **2004**, *104* (1), 293–346.

(2) Giersig, M.; Mulvaney, P. Preparation of ordered colloid monolayers by electrophoretic deposition. *Langmuir* **1993**, *9*, 3408–3413.

(3) Park, S. Y.; Lytton-Jean, A. K. R.; Lee, B.; Weigand, S.; Schatz, G. C.; Mirkin, C. A. DNA-programmable nanoparticle crystallization. *Nature* **2008**, *451* (7178), 553–556.

(4) Murphy, C. J.; Gole, A. M.; Stone, J. W.; Sisco, P. N.; Alkilany, A. M.; Goldsmith, E. C.; Baxter, S. C. Gold Nanoparticles in Biology: Beyond Toxicity to Cellular Imaging. *Acc. Chem. Res.* **2008**, *41* (12), 1721–1730.

(5) Röcker, C.; Pötzl, M.; Zhang, F.; Parak, W. J.; Nienhaus, G. U. A quantitative fluorescence study of protein monolayer formation on colloidal nanoparticles. *Nat. Nanotechnol.* **2009**, *4*, 577–580.

(6) Tkachenko, A.; Xie, H.; Liu, Y.; Coleman, D.; Ryan, J.; Glomm, W.; Shipton, M.; Franzen, S.; Feldheim, D. Cellular trajectories of peptide-modified gold particle complexes: comparison of nuclear localization signals and peptide transduction domains. *Bioconjugate Chem.* **2004**, *15* (3), 482–490.

(7) Cedervall, T.; Lynch, I.; Lindman, S.; Berggard, T.; Thulin, E.; Nilsson, H.; Dawson, K.; Linse, S. Understanding the nanoparticle-protein corona using methods to quantiify exchange rates and affinities of proteins for nanoparticles. *Proc. Natl. Acad. Sci. U.S.A.* **2007**, *104* (7), 2050–2055.

(8) Moreau, J.; Weber, P.; Martin, M.; Gilbert, B.; Hutcheon, I.; Banfield, J. Extracellular proteins limit the dispersal of biogenic nanoparticles. *Science* **2007**, *316*, 1600–1603.

(9) Kratz, F. Albumin as a drug carrier: design of prodrugs, drug conjugates and nanoparticles. *J. Controlled Release* **2008**, *132* (3), 171–183.

(10) Leo, E.; Contado, C.; Bortolotti, F.; Pavan, B.; Scatturin, A.; Tosi, G.; Manfredini, S.; Angusti, A.; Dalpiaz, A. Nanoparticle formulation may affect the stabilization of an antiischemic prodrug. *Int. J. Pharm.* **2006**, *307* (1), 103–113.

(11) Doherty, F. G. The Asiatic Clam, *Corbicula* Spp, as a biological monitor in fresh-water environments. *Environ. Monit. Assess.* **1990**, *15* (2), 143–181.

(12) Croteau, M. N.; Luoma, S. N. Delineating copper accumulation pathways for the freshwater bivalve *Corbicula* using stable copper isotopes. *Environ. Toxicol. Chem.* **2005**, *24* (11), 2871–2878.

(13) Champeau, O.; Narbonne, J. F. S. Effects of tributyltin and 17 beta-estradiol on immune and lysosomal systems of the Asian clam *Corbicula* fluminea (M.). *Environ. Toxicol. Pharmacol.* **2006**, *21* (3), 323–330.

(14) Belanger, S. E.; Cherry, D. S.; Cairns, J.; McGuire, M. J. Using Asiatic Clams as a Biomonitor for Chrysotile Asbestos in Public Water-Supplies. *J. - Am. Water Works Assoc.* **1987**, *79* (3), 69–74.

(15) Blaise, C.; Trottier, S.; Gagne, F.; Lallement, C.; Hansen, P. D. Immunocompetence of bivalve hemocytes as evaluated by a miniaturized phagocytosis assay. *Environ. Toxicol.* **2002**, *17* (3), 160–169.

(16) Graczyk, T. K.; Fayer, R.; Cranfield, M. R.; Conn, D. B. Recovery of waterborne *Cryptosporidium parvum* oocysts by freshwater benthic clams (*Corbicula fluminea*). *Appl. Environ. Microb.* **1998**, *64* (2), 427–430.

(17) Miller, W. A.; Gardner, I. A.; Atwill, E. R.; Leutenegger, C. M.; Miller, M. A.; Hedrick, R. P.; Melli, A. C.; Barnes, N. M.; Conrad, P. A. Evaluation of methods for improved detection of *Cryptosporidium* spp. in mussels (*Mytilus californianus*). *J. Microbiol. Methods* **2006**, *65* (3), 367–379.

(18) Ferry, J.; Craig, P.; Hexell, C.; Sisco, P.; Frey, R.; Pennington, P.; Fulton, M.; Scott, I.; Decho, A.; Kashiwada, S.; Murphy, C.; Shaw, T. Transfer of gold nanoparticles from the water column to the estuarine food web. *Nat. Nanotechnol.* **2009**, *4*, 441–444.

(19) Renault, S.; Baudrimont, M.; Mesmer-Dudons, N.; Gonzalez, P.; Mornet, S.; Brisson, A. Impacts of gold nanoparticle exposure on two freshwater species: a phytoplanktonic alga (*Scenedesmus subspicatus*) and a benthic bivalve (*Corbicula fluminea*). *Gold Bull.* **2008**, *41* (2), 116–126.

(20) Li-Mei, A.; Feng, G.; Bi-Feng, P.; Da-Xiang, C.; Hong-Chen, G. Interaction between gold nanoparticles and bovine serum albumin or sheep antirabbit immunoglobulin G. *Chin. J. Chem.* **2006**, *24*, 253–256.

(21) Jana, N.; Gearheart, L.; Murphy, C. Wet chemical synthesis of high aspect ratio cylindrical gold nanorods. *J. Phys. Chem. B* **2001**, *105*, 4065–4067.

(22) Turkevich, J.; Stevenson, P. C.; Hillier, J. A. Study of the nucleation and growth processes in the synthesis of colloidal gold. *Discuss. Faraday Soc.* **1951**, *11*, 55–59.

(23) Frens, G. Controlled nucleation for the regulation of the particle size in monodisperse gold suspensions. *NPHS* **1973**, *241*, 20–22.

(24) Ji, X.; Song, X.; Li, J.; Bai, Y.; Yang, W.; Peng, X. Size control of gold nanocrystals in citrate reduction: the third role of citrate. *J. Am. Chem. Soc.* **2007**, *129* (45), 13939–13948.

(25) APHA; AWWA; WEF, Standard Methods for Examination of Water and Wastewater. 1998.

(26) Laforsch, C.; Tolldrian, R. A new preparation technique for daphnids for scanning electron microscopy by using hexamethyldisilazane. *Arch. Hydrobiol.* **2000**, *149*, 587–596.

(27) Flank, A. M.; Cauchon, G.; Lagarde, P.; Bac, S.; Janousch, M.; Wetter, R.; Dubuisson, J. M.; Idir, M.; Langlois, F.; Moreno, T.; Vantelon, D. LUCIA, a microfocus soft XAS beamline. *Nucl. Instrum. Methods Phys. Res., Sect. B* **2006**, *246*, 269–274.

(28) Haiss, W.; Thanh, N.; Aveyard, J.; Fernig, D. Determination of size and concentration of gold nanoparticles from UV-Vis spectra. *Anal. Chem.* **2007**, *79*, 4215–4221.

(29) Diegoli, S.; Manciulea, A.; Begum, S.; Jones, I.; Lead, J.; Preece, J. Interaction between manufactured gold nanoparticles and naturally occurring organic macromolecules. *Sci. Total Environ.* **2008**, *402*, 51–61.

(30) Khlebtsov, N.; Dykman, L.; Krasnov, Y.; Mel'nikov, A. Light absorption by the clusters of colloidal gold and silver particles formed during slow and fast aggregation. *Colloid J.* **2000**, *62* (6), 765–779.

(31) Wiesner, M. R.; Lowry, G. V.; Alvarez, P.; Dionysiou, D.; Biswas, P. Assessing the risks of manufactured nanomaterials. *Environ. Sci. Technol.* **2006**, *40* (14), 4336–4345.

(32) Kryger, J.; Riisgard, H. Filtration rate capacities in 6 species of European freshwater bivalves. *Oecologia* **1988**, *77*, 34–38.

(33) Kennedy, A. J.; Hull, M. S.; Steevens, J. A.; Dontsova, K. M.; Chappell, M. A.; Gunter, J. C.; Weiss, C. A. Factors influencing the partitioning and toxicity of nanotubes in the aquatic environment. *Environ. Toxicol. Chem.* **2008**, *27* (9), 1932–1941.

(34) Way, C. A.; Hornbach, D. J.; Miller-Way, C. A.; Payne, B. S.; Miller, A. C. Dynamics of filter feeding in *Corbicula fluminea* (Bivalvia: Corbiculidae). *Can. J. Zool.* **1990**, *68*, 115–120.

(35) Hornbach, D. J.; Way, C. M.; Wissing, T. E.; Burky, A. J. Effects of particle concentration and season on the filtration rates of the freshwater clam, *Sphaerium striatinum* Lamarck (Bivalvia: Pisidiidae). *Hydrobiologia* **1984**, *108*, 83–96.

(36) Morton, B. Studies on the biology of Dreissena polymorpha Pall. v. Some aspects of filter-feeding and the effect of microorganisms upon the rate of filtration. *Proc. Malacol. Soc. London* **1971**, *39*, 289–301.

(37) Riisgard, H. Efficiency of particle retention and filtration rate in 6 species of Northeast American bivalves. *Mar. Ecol.: Prog. Ser.* **1988**, *45*, 217–223.

(38) Silverman, H.; Lynn, J. W.; Beninger, P. G.; Dietz, T. H. The role of the latero-frontal cirri in particle capture by the gills of *Mytilus edulis*. *Biol. Bull.* **1999**, *197*, 368–376.

(39) Mohlenberg, F.; Riisgard, H. U. Efficiency of particle retention in 13 species of suspension feeding bivalves. *Ophelia* **1978**, *17*, 239–246.

(40) Vahl, O. Efficiency of particle retention in *Mytilus edulis* L. *Ophelia* **1972**, *10*, 17–25.

(41) Ropert, M.; Goulletquer, P. Comparative physiological energetics of two suspension feeders: polychaete annelid *Lanice conchilega* (Pallas 1766) and Pacific cupped oyster *Crassostrea gigas* (Thunber 1795). *Aquaculture* **2000**, *181*, 171–189.

(42) van Sprang, H. Fundamental parameter methods in XRF spectroscopy. *Adv. X-Ray Anal.* **2000**, *42*, 1–10.

(43) Ward, J. E.; Kach, D. J. Marine aggregates facilitate ingestion of nanoparticles by suspension-feeding bivalves. *Mar. Environ. Res.* **2009**, *68*, 137–142.

(44) Haven, D. S.; Alamo, R. M. Aspects of biodeposition by oysters and other invertebrate filter feeders. *Limnol. Oceanogr.* **1966**, *11* (4), 487–498.